JOURNAL OF THEORETICAL AND APPLIED MECHANICS
48, 1, pp. 71-86, Warsaw 2010

EXPERIMENTAL MODEL OF FRACTURE OF FUNCTIONALLY GRADED MATERIALS

Mieczysław Jaroniek

Technical University of Lodz, Department of Materials and Structures Strength, Lodz, Poland
e-mail: mieczyslaw.jaroniek@p.lodz.pl

Fabrication of functionally graded materials (FGM) can be obtained by layered mixing of two materials of different thermo-mechanical properties with different volume ratios gradually changing from layer to layer such that the first layer has only a few particles of the second phase and the last has the maximum volume ratio of the first phase.
Consider a simple model of the functionally graded materials as a multi-layered beam bonded to planes having shear modulus G_i and Poisson's ratio ν_I, respectively, subjected to bending. The behaviour of cracks depends on cracks configuration, size, orientation, material properties, and loading characteristic. The fracture mechanics problem will be approached by making use of photoelastic visualisation of fracture events in the model structure.

Key words: composites, fracture mechanics, photoelastic method, finite element method, functionally graded materials

1. Introduction

AN FGM material has functionally graded thermal and stress barriers. Between the 100% ceramic layer and 100% metallic bond layer there exist a functionally graded layer 2 that contains some volume ratio of the bond (metallic) phase $V_b(y)$, as a function of the distance y from the bond layer and the rest volume ratio of the ceramic phase $V_c(y)$, also as a function of distance y from the bond layer, such that $V_b(y) + V_c(y) = 1$, where h is the thickness of the functionally graded layer.

Fabrication of the FGM can be obtained similarly by layered mixing of two photoelastic materials of different thermo-mechanical properties with different volume ratios gradually changing from layer to layer such that the first layer

has only a few particles of the other phase and the last has the maximum volume ratio of the first phase.

The development of the failure criterion for a particular application is also very important for predictions of the crack path and critical loads.

Recently, there has been a successful attempt in formulation of problems of multiple cracks without any limitation. This attempt was concluded with a series of papers summarising the undertaken research for isotropic (Cook and Erdogan, 1972), anisotropic (Gupta, 1973) and non-homogeneous class of problems, see Hilton and Sin (1971), Gupta (1973).

Crack propagation in multi-layered composites of finite thickness is especially challenging and still remains an open field for investigation. Some results have been recently reported in Hilton and Sin (1971). The numerical calculations were carried out using the finite element programs ANSYS 9 and 10 (User's..., 2006). Two different methods were used: solid modelling and direct generation.

2. Material properties

Material properties influence the stress distribution and concentration, damage process and load carrying capacity of elements. In the case of elastic-plastic materials, a region of plastic strains originates in most heavily loaded cross-sections. In order to visualise the state of strains and stresses, some tests have been performed on samples made of the "araldite"-type optically active epoxy resin (Ep-53) modified with softening agents in such a way that an elastic material has been obtained. Properties of the components of the experimental model are given in Table 1.

Table 1. Mechanical properties of components of the experimental model

Layer	Young's modulus E_i [MPa]	Poisson's ratio ν_i [–]	Photoelastic constants in terms of stress k_σ [MPa/fr]	Photoelastic constants in terms of strain f_ε [1/fr]
1	3450.0	0.35	1.68	$6.572 \cdot 10^{-4}$
2	1705.0	0.36	1.18	$9.412 \cdot 10^{-4}$
3	821.0	0.38	0.855	$14.31 \cdot 10^{-4}$
4	683.0	0.40	0.819	$16.79 \cdot 10^{-4}$

3. Experimental results

Dimensions of a typical model used in the experiment and artificially initiated small cracks in the tension zone are given in Fig. 1a.

Photoelastic models before test (under initial loading) in a circular polariscope and in a monochromatic sodium light are presented in Fig. 1b, from which we get isochromatics in the layer in the initial phase.

Isochromatics are the locus of points along which the difference in the first and second principal stress $(\sigma_1 - \sigma_2)$ remains the same.

Further, as the load was increased, the isochromatics ran parallel to the beam axis Figure 1c gives a picture of stress distribution even around abrupt discontinuities in the material (in the neighbourhood of the crack).

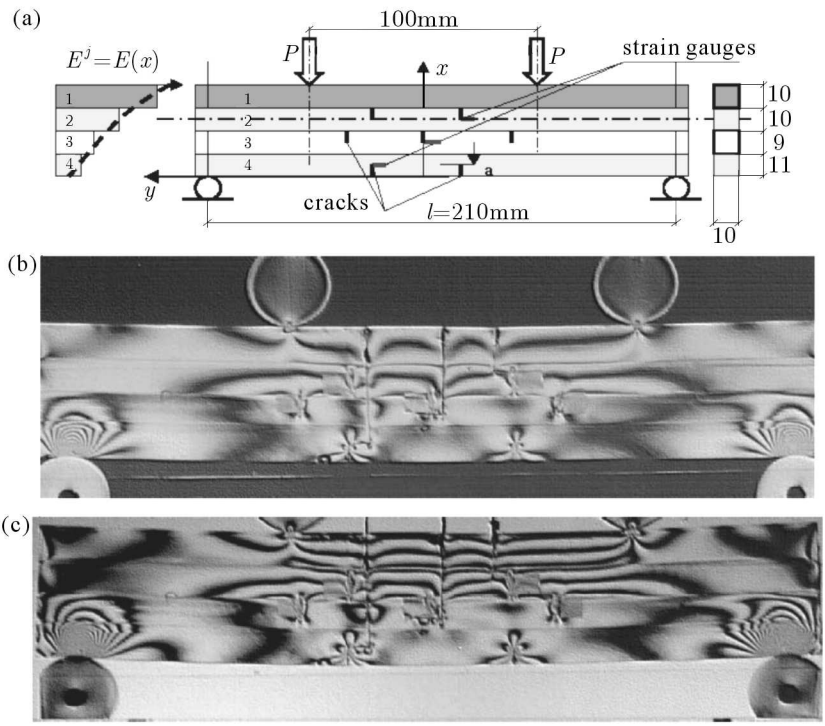

Fig. 1. (a) Four-layer beam with cracks. Photoelastic model under four point bending, isochromatic patterns $(\sigma_1 - \sigma_2)$ distribution. (b) Initial loading $(P = 20.0\,\mathrm{N})$; (c) $P = 50.0\,\mathrm{N}$ – tension of layers 2, 3 and 4

The stress distribution was determined by making use of two methods: Shear Stress Difference Procedure (SDP – evaluation of the complete stress state by means of the isochromatics and angles of isoclines along the cuts) (Frocht, 1960).

The photoelastic model of a four layer beam with cracks under four point bending, the isochromatic patterns $(\sigma_1 - \sigma_2)$ distribution corresponding to initiation of the vertical cracks and tension of overcoat (layer 4), and compression of the substrate (layer 1) are presented in Fig. 2.

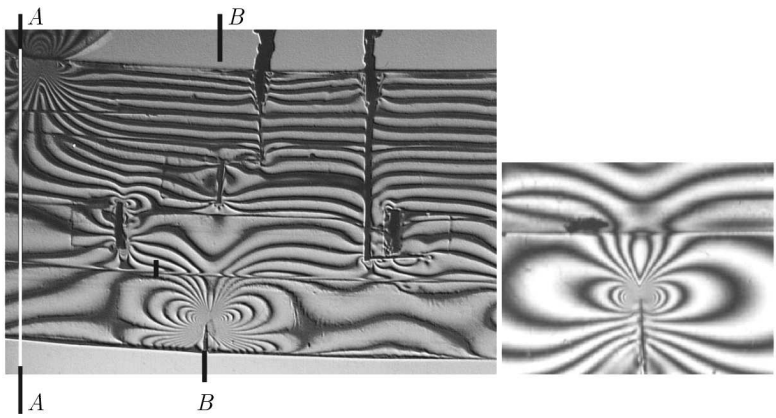

Fig. 2. Experimentally obtained isochromatic patterns $(\sigma_1 - \sigma_2)$ according to the initiation of crack propagation

The stress distribution corresponding to initiation of the vertical cracks was evaluated from measurement results of the isochromatic and isoclinic patterns according to Frocht (1960).

By means of the angles of isoclinics of isochromatics along the cuts y et $y + \Delta y$ and by employing the equations of equilibrium, the complete stress state was determined.

The stress distribution σ_x in cross sections A-A and B-B determined using the shear stress difference procedure, by means of the angles of isoclinics, is shown in Fig. 3.

Method of characteristics (stress distribution was determined using isochromatics only and equations of equilibrium (Szczepiński, 1961).

In a general case (Sanford and Dally, 1979), the Cartesian components of stress: σ_x, σ_y and τ_{xy} in the neighbourhood of the crack tip are

$$\begin{aligned}
\sigma_x &= \frac{1}{\sqrt{2\pi r}} Bigl[K_I \cos\frac{\Theta}{2}\Big(1-\sin\frac{\Theta}{2}\sin\frac{3\Theta}{2}\Big) - K_{II}\sin\frac{\Theta}{2}\Big(2+\cos\frac{\Theta}{2}\cos\frac{3\Theta}{2}\Big)\Big] + \sigma_{ox} \\
\sigma_y &= \frac{1}{\sqrt{2\pi r}}\Big[K_I \cos\frac{\Theta}{2}\Big(1+\sin\frac{\Theta}{2}\sin\frac{3\Theta}{2}\Big) + K_{II}\sin\frac{\Theta}{2}\cos\frac{\Theta}{2}\cos\frac{3\Theta}{2}\Big] \qquad (3.1) \\
\tau_{xy} &= \frac{1}{\sqrt{2\pi r}}\Big[K_I \sin\frac{\Theta}{2}\cos\frac{\Theta}{2}\cos\frac{3\Theta}{2} + K_{II}\cos\frac{\Theta}{2}\Big(1-\sin\frac{\Theta}{2}\sin\frac{2\Theta}{2}\Big)\Big]
\end{aligned}$$

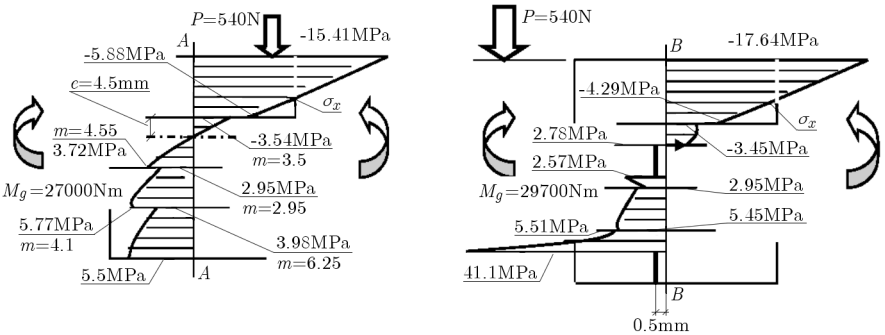

Fig. 3. Distribution of stresses in cross sections A-A and B-B (0.5 mm) with respect to the crack according to experiment and SDP evaluation

From which

$$(\sigma_1-\sigma_2)^2=\frac{1}{2\pi r}[(K_I\sin\Theta+2K_{II}\cos\Theta)^2+(K_{II}\sin\Theta)^2]+$$
$$-2\frac{\sigma_{ox}}{\sqrt{2\pi r}}\sin\frac{\Theta}{2}[K_I\sin\Theta(1+2\cos\Theta)+K_{II}(1+2\cos^2\Theta+\cos\Theta)]+\sigma_{ox}^2 \tag{3.2}$$

where K_I and K_{II} are the stress-intensity factors, r and Θ are coordinates in the polar coordinate system. By inserting the values $k_\sigma m_i=\sigma_1-\sigma_2$ into (3.2), we obtain isochromatic curves in polar coordinates (r,Θ). For each isochromatic loop, the position of maximum angle Θ_m corresponds to the maximum radius r_m. This principle can also be used in the mixed mode analysis (Sanford and Dally, 1979) by employing information from two loops in the near field of the crack, if the far field stress component $\sigma_{ox}(\Theta)=\text{const}$. Differentiating Eq. (3.2) with respect to Θ, setting $\Theta=\Theta_m$ and $r=r_m$, and substituting that $\partial\tau_m/\partial\Theta_m=0$, gives

$$g(K_I,K_{II},\sigma_{ox})=\frac{1}{2\pi r}(K_I^2\sin 2\Theta+4K_IK_{II}\cos 2\Theta-3K_{II}^2\sin 2\Theta)+$$
$$-2\frac{\sigma_{ox}}{\sqrt{2\pi rr}}\sin\frac{\Theta}{2}\Big\{[K_I(\cos\Theta+2\cos 2\Theta)-K_{II}(2\sin 2\Theta+\sin\Theta)]+$$
$$+\frac{1}{2}\cos\frac{\Theta}{2}[K_I(\sin\Theta+\sin 2\Theta)+K_{II}(2+\cos 2\Theta+\cos\Theta)]\Big\}$$
$$f(K_I,K_{II},\sigma_{ox})=(\sigma_1-\sigma_2)^2-(k_\sigma m)^2=0$$

and

$$g(K_I,K_{II},\sigma_{ox})=\frac{\partial(\sigma_1-\sigma_2)^2}{\partial\Theta_m}=0 \tag{3.3}$$

Substitution of the radii r_m and the angles Θ_m from these two loops into a pair of equations of the form given in Eq. (3.3) gives two independent relations for the parameters K_I, K_{II} and σ_{ox}. The third equation is obtained by using Eqs. (3.2). The three equations obtained that way have the form

$$\begin{aligned} &g_i(K_I, K_{II}, \sigma_{ox}) = 0 \qquad\qquad g_j(K_I, K_{II}, \sigma_{ox}) = 0 \\ &f_k(K_I, K_{II}, \sigma_{ox}) = 0 \end{aligned} \tag{3.4}$$

In order to determine K_I, K_{II} and σ_{ox}, it is sufficient to select two arbitrary points r_i, Θ_i and apply the Newton-Raphson method to the solution of three simultaneous non-linear equations (3.4). The values K_C according to mixed mode of the fracture were obtained from

$$K_C = \sqrt{K_I^2 + K_{II}^2} \tag{3.5}$$

Below are exemplary numerical results obtained from (3.4)

$$\begin{aligned} &m = 12.5 \\ &r_1 = 0.6\,\text{mm} \qquad\qquad \Theta_1 = 1.484 \\ &r_2 = 10.45\,\text{mm} \qquad\qquad \Theta_2 = 1.416 \\ &K_I^{(4)} = 0.14\,\text{MPa}\sqrt{\text{m}} \qquad\qquad K_{II}^{(4)} = 1.05\,\text{MPa}\sqrt{\text{m}} \\ &\sigma_{ox} = 0.039\,\text{MPa} \qquad\qquad K_C^{(4)} = 1.05\,\text{MPa}\sqrt{\text{m}} \end{aligned}$$

By inserting r_i, Θ_i in the three selected arbitrary points into (3.2), we obtain three non-linear equations $(i = 1, 2, 3)$

$$f_i(K_I, K_{II}, \sigma_{ox}) = 0 \tag{3.6}$$

and applying the Newton-Raphson method to the solution, we have K_I, K_{II} and σ_{ox}. Exemplary numerical results (shown in Fig. 3) obtained from (3.6) are as follows

$$\begin{aligned} &m_1 = 12.5 \qquad r_1 = 0.72\,\text{mm} \qquad \Theta_1 = 1.484 \\ &m_2 = 8.0 \qquad r_2 = 1.15\,\text{mm} \qquad \Theta_2 = 1.37 \\ &m_3 = 5.5 \qquad r_3 = 1.85\,\text{mm} \qquad \Theta_3 = 1.315 \end{aligned}$$

and

$$\begin{aligned} &K_I^{(4)} = 0.702\,\text{MPa}\sqrt{\text{m}} \qquad\qquad K_{II}^{(4)} = 1.043\,\text{MPa}\sqrt{\text{m}} \\ &\sigma_{ox} = 0.152\,\text{MPa} \qquad\qquad K_C^{(4)} = 1.257\,\text{MPa}\sqrt{\text{m}} \end{aligned}$$

4. Stress analysis from complex potentials

In the present paper, the elastic and plastic deformation has been approximately analysed using Muskhelishvili's complex potentials method

$$\sigma_{xx}+\sigma_{yy}=4\mathrm{Re}[\psi'(z)] \qquad \sigma_{yy}-\sigma_{xx}+2\mathrm{i}\tau_{xy}=2[\overline{z}\psi''(z)+\chi''(z)]$$
$$2G(u+\mathrm{i}\upsilon)=\kappa\psi(z)-z\overline{\psi}'(\overline{z})-\overline{\chi}'(\overline{z})$$
$$2G(u'+\mathrm{i}\upsilon')=\kappa\psi'(z)-z\overline{\psi}'(\overline{z})-z\overline{\psi''(z)}-\overline{\chi}''(\overline{z})$$

where $\kappa=3-4\nu$ for the plain strain and $\kappa=(3-\nu)/(1+\nu)$ for the plain stress

$$\sigma_{xx}+\sigma_{yy}=4\mathrm{Re}[\psi'(z)] \qquad \sigma_{yy}-\sigma_{xx}=\mathrm{Re}2[\overline{z}\psi''(z)+\chi''(z)]$$
$$\tau_{xy}=\mathrm{Im}[\overline{z}\psi''(z)+\chi''(z)]$$

The elastostatic stress field is required to satisfy the well-known equilibrium equations (Cherepanov, 1979) using two analytical functions $\psi(z)$ and $\chi(z)$

$$\sigma_{xx}=\mathrm{Re}[2\psi'(z)-\overline{z}\psi''(z)-\chi''(z)] \qquad \sigma_{yy}=\mathrm{Re}[2\psi'(z)+\overline{z}\psi''(z)+\chi''(z)]$$
$$\tau_{xy}=\mathrm{Im}[\overline{z}\psi''(z)+\chi''(z)] \qquad \chi''(z)=-z\psi''(z) \tag{4.1}$$
$$2G(u+\mathrm{i}\upsilon)=\kappa\psi(z)-z\overline{\psi}'(z)-\overline{\chi}'(z)$$

Using these two analytical functions $\psi(z)$ and $\chi(z)$

$$\psi'(z)=\psi_1'(z)+\psi_2'(z) \qquad \chi''(z)=z[\psi_1''(z)-\psi_2''(z)]$$

The stresses are assumed as follows

$$\sigma_x=\mathrm{Re}[2\psi'-2x\psi_1'']-y\mathrm{Im}2\psi_2'' \qquad \sigma_y=\mathrm{Re}[2\psi'+2x\psi_1'']+y\mathrm{Im}2\psi_2''$$
$$\tau_{xy}=x\mathrm{Im}2\psi_1''-y\mathrm{Re}2\psi_2'' \tag{4.2}$$

The stress-intensity factors are related by

$$K_I=\lim_{x\to a}\sigma_y(x,0)\sqrt{2\pi(x-a)} \qquad K_{II}=\lim_{x\to a}\tau_{xy}(x,0)\sqrt{2\pi(x-a)} \tag{4.3}$$

By inserting (4.2) into (4.3), we obtain

$$K_I^{(j)}=\lim_{x\to a}\{\mathrm{Re}[2\psi'^{(j)}(z)]+x2\psi''^{(j)}(z)\}\sqrt{2\pi(x-a)}$$
$$K_{II}^{(j)}=\lim_{x\to a}\{x\mathrm{Im}[2\psi^{(j)}(z)]\}\sqrt{2\pi(x-a)}$$

The complex stress potentials are assumed as follows

$$\begin{aligned} 2\psi^{j}(z) &= \sum_{n=1}^{N}\Big(C_n \int z^{(2-n)}\sqrt{\frac{z-a}{z+a}}\,dz\Big) \\ 2\psi^{'(j)}(z) &= \sum_{n=1}^{N}\sqrt{\frac{z-a}{z+a}}C_n^j z^{(2-n)} \end{aligned} \tag{4.4}$$

In this case, the Cartesian components of the stresses σ_x, σ_y and τ_{xy} are given as

$$\begin{aligned} \sigma_x^j &= \sum_{n=1}^{N}\{\mathrm{Re}[(\overline{C}_n^j + \mathrm{i}\overline{\overline{C}}_n^j)f_1(z)]\} \qquad \sigma_y^j = \sum_{n=1}^{N}\{\mathrm{Re}[(\overline{C}_n^j + \mathrm{i}\overline{\overline{C}}_n^j)f_4(z)]\} \\ \tau_{xy}^j &= \sum_{n=1}^{N}\{x\mathrm{Im}[(\overline{C}_n^j + \mathrm{i}\overline{\overline{C}}_n^j)f_5(z)]\} \end{aligned} \tag{4.5}$$

where

$$\begin{aligned} f_1(z) &= \frac{1}{z^{n-1}}\Big(\frac{1}{z}\sqrt{\frac{z-a}{z+a}} - x\frac{az-(n-2)(z^2-a^2)}{(z+a)\sqrt{z^2-a^2}}\Big) \\ f_2(z) &= \frac{z^{3-n}}{\sqrt{z^2-a^2}} \\ f_3(z) &= z^{2-n}\frac{(3-n)(z^2-a^2)+z^2}{(z^2-a^2)^{3/2}} \\ f_4(z) &= \frac{1}{z^{n-1}}\Big(\frac{1}{z}\sqrt{\frac{z-a}{z+a}} + x\frac{az-(n-2)(z^2-a^2)}{(z+a)\sqrt{z^2-a^2}}\Big) \\ f_5(z) &= \frac{1}{z^{n-1}}\frac{az(n-2)(z^2-a^2)}{(z+a)\sqrt{z^2-a^2}} \end{aligned}$$

and

$$\begin{aligned} C_n^i &= \mathrm{Re}C_n^i + \mathrm{i}\mathrm{Im}C_n^i \qquad \overline{C}_n^i = \mathrm{Re}C_n^i \\ D_n^i &= \mathrm{Re}D_n^i + \mathrm{i}\mathrm{Im}D_n^i \qquad \overline{\overline{C}}_n^i = \mathrm{Im}C_n^i \end{aligned} \tag{4.6}$$

The boundary conditions can be expressed as

$$\begin{aligned} \sigma_y^{(\infty)} - \sigma_x^{(\infty)} + 2\mathrm{i}\tau_{xy}^{(\infty)} &= 2\mathrm{i}y\cdot 2\psi(z) \\ \sigma_y^j = E_j\frac{(x_0-x_j)}{\rho} &= \sigma_y^{\infty} \qquad \sigma_x^{\infty} = 0 \end{aligned} \tag{4.7}$$

$$\begin{aligned} &\varepsilon_y^j = \varepsilon_y^{j+1} && \varepsilon_y^j = \frac{\partial \upsilon^j}{\partial y} && \varepsilon_x^j = \varepsilon_x^{j+1} \\ &u' = \frac{\partial u}{\partial x} && u^j = u^{j+1} && \upsilon^j = \upsilon^{j+1} \end{aligned} \tag{4.8}$$

and

$$\begin{aligned} &\int_0^H \sigma_y^j \, dx = \sum_{n=1}^{N} \Big\{ \mathrm{Re} \int_0^H \Big[\frac{C_n^j}{z^{n-1}} \Big(\frac{1}{z} \sqrt{\frac{z-a}{z+a}} + x \frac{az - (n-2)(z^2-a^2)}{(z+a)\sqrt{z^2-a^2}} \Big) \Big] \, dx \Big\} = 0 \\ &\int_0^H b\sigma_y^j x \, dx + M = \\ &\quad = \sum_{n=1}^{N} \Big\{ \int_0^H b \mathrm{Re} \Big[\frac{C_n^j}{z^{n-1}} \Big(\frac{1}{z} \sqrt{\frac{z-a}{z+a}} + x \frac{az - (n-2)(z^2-a^2)}{(z+a)\sqrt{z^2-a^2}} \Big) \Big] \, dx \Big\} + M = 0 \\ &\sigma_y^j = \sum_{n=1}^{N} \Big\{ \mathrm{Re} \Big[\frac{C_n^j}{z^{n-1}} \Big(\frac{1}{z} \sqrt{\frac{z-a}{z+a}} + x \frac{az - (n-2)(z^2-a^2)}{(z+a)\sqrt{z^2-a^2}} \Big) \Big] \Big\} \\ &\sigma_y^j = E_j \frac{(x_0 - x_i)^p}{\rho} = \sigma_y^\infty \end{aligned} \tag{4.9}$$

For each isochromatic loop $\sigma_1 - \sigma_2 = k_\sigma m$ and

$$\sigma_{yy} - \sigma_{xx} = k_\sigma m \cos 2\alpha \tag{4.10}$$

in other hand $\sigma_1 + \sigma_2 = \sigma_{xx} + \sigma_{yy}$ and

$$\sigma_{xx} + \sigma_{yy} = \sum_{n=1}^{N} 2\mathrm{Re} \Big[C_n z^{(2-n)} \sqrt{\frac{z-a}{z+a}} + \frac{D_n z^{(3-n)}}{\sqrt{z^2-a^2}} \Big] \tag{4.11}$$

This principle can be used in the analysis of stresses. By inserting values of m_i, α_i in arbitraily selected points $P(r_i, \Theta_i)$, we obtain equations

$$\sum_{n=1}^{N} \{ \mathrm{Re}[(\overline{C}_n + \mathrm{i}\overline{\overline{C}}_n)(f_4(z) - f_1(z))] + 2y\mathrm{Im}[(\overline{D}_n + \mathrm{i}\overline{\overline{D}}_n) f_3(z)] \} = k_\sigma m_i \cos 2\alpha_i \tag{4.12}$$

from which

$$\begin{aligned} &\sigma_{yy} - \sigma_{xx} = \mathrm{Re} 2[\overline{z}\psi''(z) + \chi''(z)] \\ &\tau_{xy} = \mathrm{Im}[\overline{z}\psi''(z) + \chi''(z)] \\ &\tau_m^2 = \mathrm{Re}[\overline{z}\psi''(z) + \chi''(z)]^2 + \mathrm{Im}[\overline{z}\psi''(z) + \chi''(z)]^2 \end{aligned}$$

and

$$\tau_m^2 = \Big\langle \sum_{n=1}^{N} \{x\mathrm{Re}[C_n f_5(z)] + y\mathrm{Im}[D_n f_3(z)]\} \Big\rangle^2 + \\ + \Big\langle \sum_{n=1}^{N} \{x\mathrm{Im}[C_n f_5(z)] - y\mathrm{Re}[D_n f_3(z)]\} \Big\rangle^2 \tag{4.13}$$

For each isochromatic loop

$$\varepsilon_{yy} - \varepsilon_{xx} = \\ = \frac{1}{2G'} \sum_{n=1}^{N} \{\mathrm{Re}[(\overline{C}_n + \mathrm{i}\overline{\overline{C}}_n)(f_4(z) - f_1(z))] + 2y\mathrm{Im}[(\overline{D}_n + \mathrm{i}\overline{\overline{D}}_n) f_3(z)]\} \tag{4.14}$$

in other hand

$$\varepsilon_{yy} - \varepsilon_{xx} = f_\varepsilon(m) m \cos 2\alpha \tag{4.15}$$

and

$$\frac{(1+\nu_j)}{E_j} \sum_{n=1}^{N} \{\mathrm{Re}[(\overline{C}_n^j + \mathrm{i}\overline{\overline{C}}_n^j)(f_4(z) - f_1(z))] + 2y\mathrm{Im}[(\overline{D}_n^j + \mathrm{i}\overline{\overline{D}}_n^j) f_3(z)]\} = \\ = f_\varepsilon m(x_t) \cos 2\alpha \tag{4.16}$$

By inserting the principal stress difference $m_i = (\sigma_1 - \sigma_2)_i$, the values of α_i in n arbitrarily selected points $P_i(r_i, \Theta_i)$ into (4.16), we obtain n-linear equations $(i = 1, 2, \ldots, n)$ from which we obtain values of $C_1, C_2, \ldots, C_n, D_1, D_2, \ldots, D_n$ and from (4.7) and (4.8) Cartesian components of the stress σ_x, σ_y and τ_{xy}. By inserting C_n, D_n into (4.13), we obtain isochromatic curves in the polar coordinates (r, Θ).

The distribution of isochromatic patterns $(\sigma_1 - \sigma_2)$ obtained experimentally according to crack propagation is shown in Fig. 4a and the isochromatics calculated from (4.13) according to C_n and D_n in the analysis of complex potentials are presented in Fig. 4b.

The stress-intensity factors from (9) are related by

$$K_I = \lim_{x \to a} \sum_{n=1}^{N} \Big\{ \mathrm{Re}\Big[\frac{C_n}{z^{n-1}} \Big(\frac{1}{z} \sqrt{\frac{z-a}{z+a}} + x \frac{az - (n-2)(z^2 - a^2)}{(z+a)\sqrt{z^2 - a^2}} \Big) + \frac{D_n z^{3-n}}{\sqrt{z^2 - a^2}} \Big] \cdot \\ \cdot \sqrt{2\pi(x-a)} \Big\} \\ K_{II} = \lim_{x \to a} \sum_{n=1}^{N} \Big\{ x\mathrm{Im}\Big[\frac{C_n}{z^{n-1}} \frac{az(n-2)(z^2 - a^2)}{(z+a)\sqrt{z^2 - a^2}} \Big] \sqrt{2\pi(x-a)} \Big\} \tag{4.17}$$

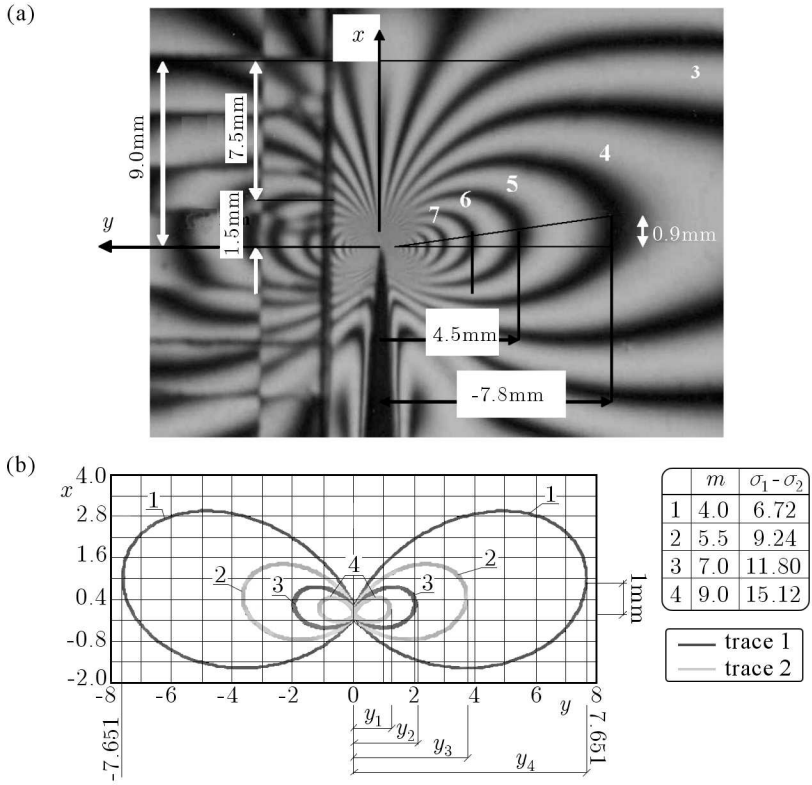

	m	σ_1-σ_2
1	4.0	6.72
2	5.5	9.24
3	7.0	11.80
4	9.0	15.12

Fig. 4. Experimentally found isochromatic patterns $(\sigma_1 - \sigma_2)$ according to crack propagation used in analysis of complex potentials

where in the polar coordinates (r, Θ)

$$z^l \sqrt{\frac{z-a}{z+a}} = r^l \sqrt{\frac{r_1}{r_2}} \Big[\cos\Big(\frac{\Theta_1+\Theta_2}{2} + \Theta l\Big) + \mathrm{i}\sin\Big(\frac{\Theta_1+\Theta_2}{2} + \Theta l\Big)\Big]$$
$$\frac{z^l}{\sqrt{z^2-a^2}} = \frac{r^l}{\sqrt{r_1 r_2}} \Big[\cos\Big(\Theta l - \frac{\Theta_1+\Theta_2}{2}\Big) + \mathrm{i}\sin\Big(\Theta l - \frac{\Theta_1+\Theta_2}{2}\Big)\Big] \tag{4.18}$$

5. Numerical determination of stress distribution

The distribution of stresses and displacements has been calculated using the finite element method (FEM) (User's..., 2006; Zienkiewicz, 1971). Finite element calculations were performed in order to verify the experimentally obse-

rved isochromatic distribution during cracks propagation. The geometry and materials of models were chosen to correspond with specimens used at present experiments. The numerical calculations were carried out using the finite element program ANSYS 9 and by applying the substructure technique.

A finite element mesh of the model (used for numerical simulation) are presented in Fig. 5.

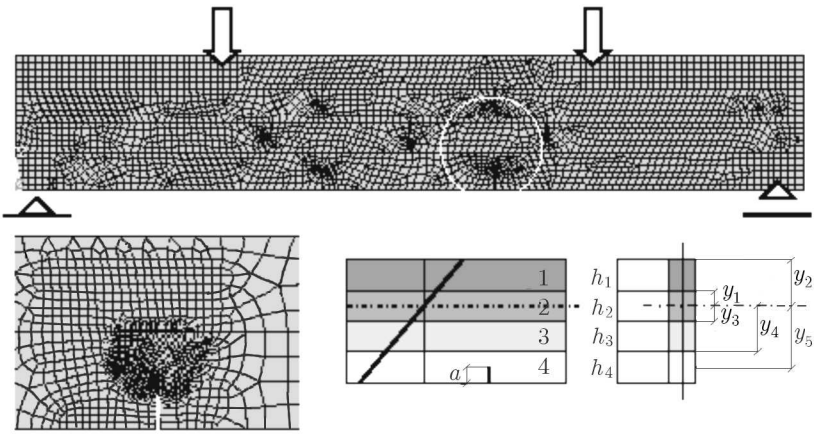

Fig. 5. Finite element mesh of the model (for numerical simulation)

The numerical (from FEM) distribution of isochromatic fringes $(\sigma_1 - \sigma_2)$ is shown in Fig. 6 and the distribution of stress σ_y obtained numerically is given in Fig. 7.

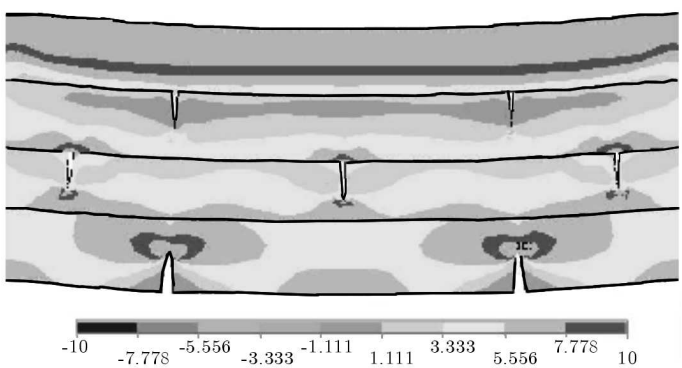

Fig. 6. Numerically obtained distribution of isochromatic patterns $(\sigma_1 - \sigma_2)$ according to crack propagation

For comparison, the distribution of isochromatic fringes $(\sigma_1 - \sigma_2)$ obtained experimentally according to the initiation of crack propagation is shown in Fig. 8.

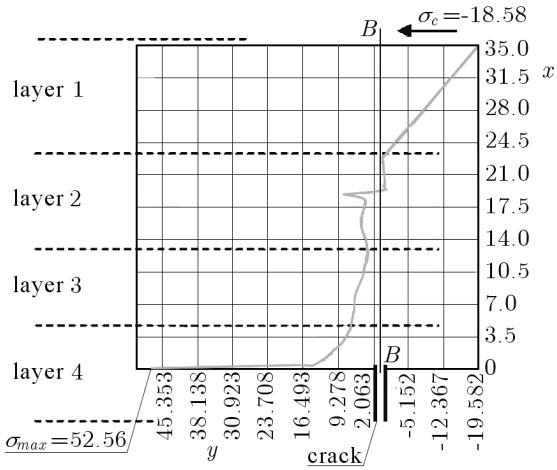

Fig. 7. Numerical determination of stress distribution (Ansys 9). Distribution of stresses σ_y along the crack

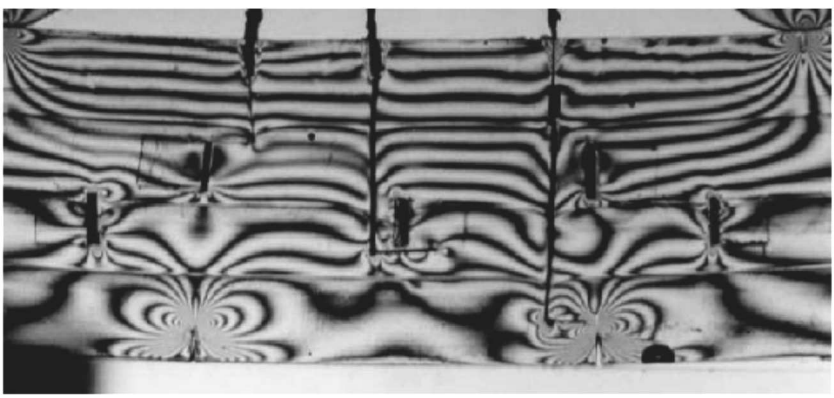

Fig. 8. Experimentall obtained distribution of isochromatic patterns $(\sigma_1 - \sigma_2)$ according to crack propagation

Table 2. Experimental and numerical results. Critical values $K_{IC}^{(4)}$ and $K_{IIC}^{(4)}$ according to crack propagation

Crack length	Critical force	Experimental results				Numerical results
a	P_{cr}	$K_I^{(4)}$	$K_{II}^{(4)}$	$K_C^{(4)}$	σ_{0x}	$K_{Cn}^{(4)}$
[mm]	[N]	[MPa$\sqrt{\text{m}}$]			[MPa]	[MPa$\sqrt{\text{m}}$]
6.0	265.0	1.177	0.8793	**1.419**	2.58	**1.45**
9.0	205.0	0.702	1.043	**1.257**	0.152	**1.28**
9.8	185.0	0.14	1.05	**1.05**	0.039	**1.16**

6. Conclusions

Formulation of the model of an FGM can be obtained similarly as the functionally graded materials themselves by layered mixing of two photoelastic materials of different thermo-mechanical properties with different volume ratios gradually changing from one layer to another such that the first layer has only a few particles of the second one and the second has the maximum volume ratio of first layer.

Photoelasticity has been shown to be promising in stress analysis of beams with various numbers and orientation of cracks.

In the present paper, the stresses and displacements have been approximately analysed using the Muskhelishvili complex potential method. Using two analytical functions, we obtained equations for the isochromatic loop.

It is possible to create a model using various photoelastic materials to model a multi-layered structure.

Finite element calculations (FEM) were performed in order to verify the experimentally observed branching phenomenon and the isochromatic distribution observed during crack propagation. The agreement between the distributions of isochromatic fringe patterns found numerically by FEM and determined photoelastically was found to be within 5-8 percent.

Having used the stress-intensity-factor criterion, the critical value of stress and deformation fields characterises the fracture toughness.

References

1. Cherepanov G.P., 1979, *Mechanics of Brittle Fracture*, McGraw-Hill, New York
2. Cook T.S., Erdogan F., 1972, Stresses in bonded materials with a crack perpendicular to the interface, *International Journal of Engineering Science*, **10**, 677-697
3. Frocht M.M., 1960, *Photoelasticity*, John Wiley, New York
4. Gupta A.G., 1973, Layered composite with a broken laminate, *International Journal of Solids and Structures*, **36**, 1845-1864
5. Hilton P.D., Sin G.C., 1971, A laminate composite with a crack normal to interfaces, *International Journal of Solids and Structures*, **7**, 913
6. Neimitz A., 1998, *Mechanics of Fracture*, PWN Warsaw [in Polish]

7. RYCHLEWSKA J., WOŹNIAK C., 2006, Boundary layer phenomena in elastodynamics of functionally graded laminates, *Archives of Mechanics*, **58**, 4/5, 431-444

8. SANFORD R.J., DALLY J., 1979, A general method for determining mixed-mode stress intensity factors from isochromatic fringe patterns, *Engineering of Fracture Mechanics*, **2**, 621-633

9. STUPNICKI J., 1965, Trends of experimental mechanics, *Journal of Theoretical and Applied Mechanics*, **34**, 2, 207-233

10. SZCZEPIŃSKI W., 1961, A photoelastic method for determining stresses by means isochromes only, *Archiwes of Applied Mechanics*, **13**, 5

11. SZYMCZYK J., WOŹNIAK C., 2006, Continuum modelling of laminates with a slowly graded microstructure, *Archives of Mechanics*, **58**, 4/5, 445-458

12. User's Guide ANSYS, 2006, 9, 10, Ansys, Inc., Huston, USA

13. WOŹNIAK C., 1993, Nonlinear macro-elastodynamics of microperiodic composites, *Bull. Ac. Pol. Sci.: Tech. Sci.*, **41**, 315-321

14. WOŹNIAK C., 1995, Microdynamics: continuum. Modelling the simple composite materials, *Journal of Theoretical and Applied Mechanics*, **33**, 267-289

15. ZIENKIEWICZ O.C., 1971, *The Finite Element Method in Engineering Science*, McGraw-Hill, London, New York

Eksperymentalny model pękania materiału funkcjonalnie zmiennego

Streszczenie

Sposób wykonania materiałów funkcyjnie zmiennych – FGM, polega na nakładaniu (lub napylaniu) kolejnych (możliwie cienkich) warstw. Warstwy te składają się zazwyczaj z dwóch składników o różnych własnościach (mechanicznych, termicznych itp.) np. ciekły metal (plazma) i ceramika. Technologia wykonania jest następująca: najpierw nakłada się warstwę czystego ciekłego metalu, następnie warstwę ciekłego metalu z niewielką domieszką ceramiki, następne warstwy to ciekły metal ze zwiększającą się ilością ceramiki, aż do ostatniej warstwy składającej się z czystej ceramiki. W ten sposób (po zastygnięciu) otrzymuje się powłoki izolacyjne stosowane do komór spalania silników, warstwy termoizolacyjne promów i kapsuł kosmicznych itp.

W pracy podano metodę doświadczalno-obliczeniową stanu naprężeń i odkształceń dla kompozytów warstwowych zbudowanych z materiałów gradientowych. Podano także dla takich kompozytów ze szczelinami kryterium zniszczenia. Opracowana metoda jest metoda hybrydową – opierając się na wynikach badań doświadczalnych, opisano stan naprężenia i odkształcenia, stosując metodę potencjałów zespolonych.

Na podstawie wyników badań doświadczalnych opisano stan naprężeń i odkształceń dla materiałów liniowo-sprężystych i sprężysto-plastycznych w formie funkcji potencjałów zespolonych. Zastosowanie metody potencjałów zespolonych w postaci szeregów do analizy pól naprężeń umożliwia analizę wyników badań doświadczalnych modeli kompozytów, z uwagi na budowę równań, które w kompleksowy sposób opisują stan naprężenia w formie sumy i różnicy naprężeń normalnych.

Przeprowadzone obliczenia i badania mają na celu weryfikację modelu, który można zastosować do obliczeń kompozytów warstwowych.

Manuscript received March 13, 2009; accepted for print April 20, 2009